Journal of Thermal Analysis, Vol. 49 (1997) 57-70

Polymers

MODULATED DIFFERENTIAL SCANNING CALORIMETRY IN THE GLASS TRANSITION REGION VI. Model calculations based on poly(ethylene terephthalate)

*B. Wunderlich and I. Okazaki**

Department of Chemistry, The University of Tennessee, Knoxville, TN 37996-1600 and Chemical and Analytical Sciences Division, Oak Ridge National Laboratory, Oak Ridge TN 37831-6197, USA

Abstract

Temperature-modulated calorimetry (TMC) allows the experimental evaluation of the kinetic parameters of the glass transition from quasi-isothermal experiments. In this paper, model calculations based on experimental data are presented for the total and reversing apparent heat capacities on heating and cooling through the glass transition region as a function of heating rate and modulation frequency for the modulated differential scanning calorimeter (MDSC). Amorphous poly(ethylene terephthalate) (PET) is used as the example polymer and a simple first-order kinetics is fitted to the data. The total heat flow carries the hysteresis information (enthalpy relaxation, thermal history) and indications of changes in modulation frequency due to the glass transition. The reversing heat flow permits the assessment of the first and higher harmonics of the apparent heat capacities. The computations are carried out by numerical integrations with up to 5000 steps. Comparisons of the calculations with experiments are possible. As one moves further from equilibrium, i.e. the liquid state, cooperative kinetics must be used to match model and experiment.

Keywords: enthalpy relaxation, glass transition, heat capacity, heat flow calorimeter, hysteresis, poly(ethylene terephthalate), temperature-modulated calorimetry, TMC

Introduction

The kinetics of the glass transition has been a topic of long-standing interest. In the past, most data were collected with mechanical and dielectric probes [1]. Only

* On leave from Toray Industries, Inc., Otsu, Shiga 520, Japan.

0368–4466/97/ $ 5.00

John Wiley & Sons Limited
Chichester

one early investigation of the kinetics of the glass transition was based on calorimetry (dynamic differential thermal analysis, DDTA) [2]. The model calculations of this paper are based on temperature-modulated calorimetry (TMC). Specifically, a temperature-modulated differential scanning calorimetry (TMDSC) of the heat-flux type was used to generate the parameters for the modeling (Modulated DSC of TA Instruments, MDSC™).

The modulated temperature consists in MDSC of a sinusoidal oscillation superimposed on an underlying heating rate $dT/dt = <q>$ [3]. At steady state the sample temperature is [4]:

$$T_s(t) = T_o + <q>t - <q>\frac{C_s}{K} + A\ \sin(\omega t - \varepsilon) \qquad (1)$$

where T_o is the temperature at the start of the experiment; C_s, the heat capacity of the sample calorimeter (sample+pan); K, the Newton's law constant [5]; A, the maximum amplitude of the sample-temperature modulation; ω, the modulation frequency $2\pi/p$ (p=modulation period in seconds); and ε is the phase shift relative to the temperature oscillation of the heater (block). An analogous equations holds for the reference temperature, T_r (maximum amplitude A_r and phase shift φ). The temperature difference, $\Delta T = T_r - T_s$ (maximum amplitude A_Δ and phase shift δ) is proportional to the heat flow (*HF*).

Measurements with TMDSC have two time scales, one due to the underlying heating rate and one due to the modulation. As soon as the heat capacity becomes time-dependent (apparent heat capacity), the two time scales cause different effects on the measurement. The separation of the effects due to the underlying heating rate and the modulation are the main topic of the paper. The computations made use of data on amorphous poly(ethylene terephthalate) (PET).

The heat capacity due to the modulation, the "reversing" heat capacity, is separated from the "total heat capacity" due to the underlying heating rate $<q>$ by a pseudo-isothermal analysis. The change in ΔT at time t due to modulation alone is approximated by $\Delta T(t) - <\Delta T>$ with the average taken over $t \pm p/2$. Evaluation of the calibration constant and the maximum amplitude of the temperature difference, A_Δ, which is proportional to the maximum heat flow amplitude A_{HF}, gives the "reversing" heat capacity as long as the temperature gradient within the sample is negligible and steady state has been achieved [4]:

$$mc_p = \frac{A_\Delta}{A}\sqrt{\left(\frac{K}{\omega}\right)^2 + C'^2} = \frac{A_{HF}}{A} \times K' \qquad (2)$$

where A and ω are parameters set at the beginning of the experiment, and C' is the heat capacity of the empty reference pan of identical mass to the empty sample pan. The calibration constant K is independent of modulation frequency and reference heat capacity. The commonly measured calibration constant K' changes for runs with different ω and C'. The "total heat capacity," in turn, is extracted from the data without the modulation effects by appropriate averaging:

$$mc_p^{total} \approx \frac{K<\Delta T>}{<q>} = \frac{K''<HF>}{<q>} \tag{3}$$

where K is the same Newton's law constant as in Eq. (20). In case the heat capacity at a given temperature is independent of time, Eqs (2) and (3) give the same result.

The conditions for the approach of the calorimeter to steady state have been explored [6] and it was shown that small samples can at present be studied by TMDSC over about one order of magnitude of change in time scale [7]. The parameters for the description of the time-dependence of the heat capacity of PET were evaluated by quasi-isothermal, frequency-dependent, measurements of the "reversing" heat capacity [8] [$<q>=0$ in Eq. (1)]. Details are presented in [9]. Comparisons of calculations using irreversible thermodynamics, linked to the hole-theory of liquids as described in [2] with experiments have shown agreement, as long as the maximum modulation amplitude is small (≈0.1 K) and the distance in temperature from the equilibrium melt is small (≈5 K). An approximate correspondence is maintained at larger distances from equilibrium and at larger amplitudes [10]. In the present paper data are computed that extend beyond the limits of present experimentation and permit predictions of possible future applications. Furthermore the results help to gain a better understanding of the "reversing" c_p.

Details of the simulations

Computation of the MDSC output from a given heat flow

To link any computed heat flow to the expected output from the calorimeter, the commercial software of data analysis by the modulated DSC of TA Instruments, MDSC™, was modeled with the Lotus 1-2-3™ spread sheet (Version 4), assuming steady state was maintained and a negligible temperature gradient exists within the sample [11]. Briefly, the instantaneous amplitudes of the heat flow at t, $HF(t)$, is used to compute the Fourier components that are out-of-phase and in-phase with the reference modulation sin ωt at the heater:

$$HF_{cos}(t) = [HF(t) - <HF(t)>] \cos\omega t \qquad [= A_{HF} \sin(\omega t - \delta) \cos\omega t] \tag{4}$$

$$HF_{sin}(t) = [HF(t) - <HF(t)>] \sin\omega t \qquad [= A_{HF} \sin(\omega t - \delta) \sin\omega t] \tag{5}$$

where the average $<HF(t)>$ is taken over one modulation period and can be used to compute the "total" heat capacity using Eq. (3). If t_1, t_2, and t_3 are the times defining successive intervals of $p/2$ in direction from the last to the first measured point, and n is the number of points determined per cycle, the average at t_2 is given by:

$$<HF(t_2)> = \frac{1}{n}\sum_{t_3}^{t_5} HF(t) \tag{6}$$

The difference $[HF(t)-<HF(t)>]$ in Eqs (4) and (5) represents the modulation amplitude without the effect of the underlying heating rate $<q>$, i.e. Eqs (4) and (5)

simulate a pseudo-isothermal analysis of the experiment described by Eq. (1). The second parts of Eqs (4) and (5), written in brackets, represent the corresponding mathematical equivalents of the components of the modulated heat flow with a phase-shifted response. This is followed by further averaging (integrating) over one full period p:

$$<HF_{cos}(t_2)> = \frac{\sum_{t_3}^{t_1} HF_{cos}(t)}{n} \qquad [= <A_{HF}/2 \sin\delta>] \tag{7}$$

$$<HF_{sin}(t_2)> = \frac{\sum_{t_3}^{t_1} HF_{sin}(t)}{n} \qquad [= <A_{HF}/2 \cos\delta>] \tag{8}$$

The equations in brackets are obtained by integration of the bracketed Eqs (4) and (5). Simple vector addition of Eqs (7) and (8) gives then the maximum amplitude of modulation of HF:

$$<A_{HF}(t_2)> = 2\sqrt{<HF_{sin}(t_2)>^2 + <HF_{cos}(t_2)>^2} \tag{9}$$

which can be used to calculate the "reversing" heat capacity, using Eq. (2).

Equation (6) is also the constant b_0 when expressing the heat flow as a Fourier series with period p:

$$HF(t) = b_0 + \sum_{\nu=1}^{\nu=\infty}\left[a_\nu \sin\frac{2\pi\nu}{p}t + b_\nu \cos\frac{2\pi\nu}{p}t\right] \tag{10}$$

The constant b_0 and the maximum amplitudes a_ν and b_ν are given by:

$$b_0 = \frac{1}{p}\int_{-p/2}^{+p/2} HF(t)\mathrm{d}t \tag{11}$$

$$a_\nu = \frac{1}{2p}\int_{-p/2}^{+p/2} HF(t)\sin\left(\frac{2\pi\nu}{p}t\right)\mathrm{d}t \tag{12}$$

$$b_\nu = \frac{1}{2p}\int_{-p/2}^{+p/2} HF(t)\cos\left(\frac{2\pi\nu}{p}t\right)\mathrm{d}t \tag{13}$$

where ν is a running integer starting from 1. Equations (7) and (8) correspond then to the coefficients b_1 and a_1, representing the first harmonics of the Fourier series; and b_0 is the total heat flow $<HF(t)>$. The analysis can easily be extended to the

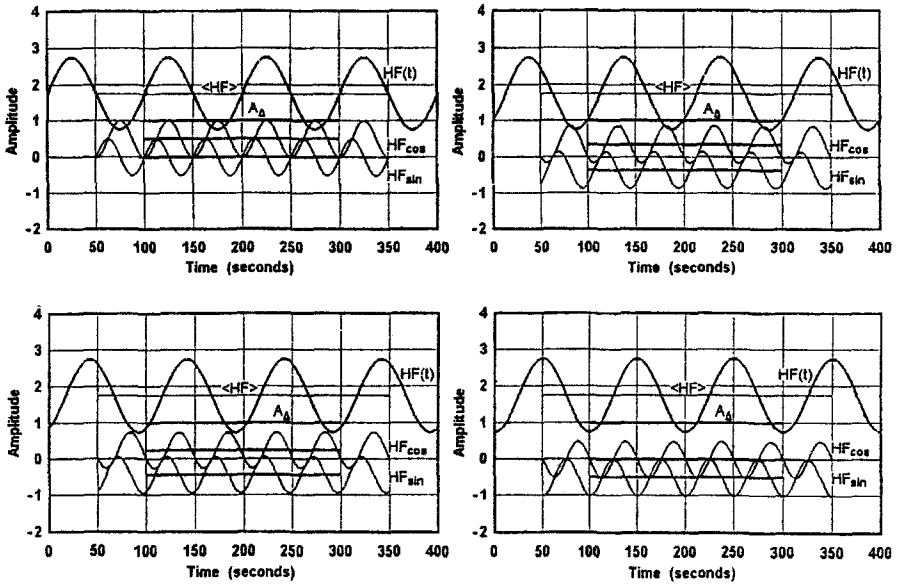

Fig. 1 Sinusoidal heat flow with different phase lags analyzed by a simulation duplicating the MDSC software, as described in Ref. [11]. The shorter time intervals for all data but the total heat flow *HF(t)* indicate the restrictions due to the calculations of Eqs (4) to (8). Further smoothing of the output A_Δ, as done in the MDSC software, would limit the information gained from the 400 s interval of data for heat flow to 100 s (150 to 250 s)

second, third, and higher harmonics by using $v\omega t$ in Eqs (4) and (5) with $v=2$, 3, and higher, respectively.

Figure 1 illustrates the analysis of the amplitude *HF(t)* in the presence of a constant heat flow $<HF>$ of 1.75, a modulation period of 100 s, and a maximum modulation amplitude A_Δ of 1.00 for phase shift values relative to ωt of $\delta=0$, $\pi/4$, $\pi/3$ and $\pi/2$. The heat capacities could be computed from either $<HF>$ or A_Δ, using Eqs (2) or (3). Both values would be identical for reversing changes in the given time frame. Figure 1 shows also the components of Eqs (4) and (5) as a function of the phase shift δ. For the other three quadrants of the phase shift, corresponding sine and cosine components result. The integral expressions of Eqs (7) and (8) are the lower two bolded horizontals, and their vector sum, given by Eq. (9), results in the expected $<HF>$. The output of Eq. (9) from the MDSC software is smoothed further by averaging once more [6, 11]. To enable a more detailed analysis of the influence of the glass transition kinetics, this final smoothing is omitted in all the simulations presented in this paper.

In the next section it will be shown how in the glass transition region the heat flow is altered. The Results section will then show the expected apparent heat capacities under various modulation frequency, distance from equilibrium, and underlying heating rate when using the just summarized simulation of the MDSC analysis.

Kinetics of the glass transition and its simulation

In the liquid state, longer times are necessary to reach thermal equilibrium than in the solid because of the need of the molecules to undergo larger, cooperative, structural changes. A simple model for the representation of these motions has been given in terms of the hole theory, i.e. the larger expansivity of liquids and the slower response to changes in temperature are assumed to be due to changes in an equilibrium of holes. The equilibrium number of holes is N^*, each contributing an energy ε_h to the enthalpy. The hole contribution to the heat capacity is then given by the change in number of holes with temperature under equilibrium conditions, so that the heat capacity is [2]:

$$C_p(\text{liquid}) = C_{p_o} + \varepsilon_h \left(\frac{dN^*}{dT}\right) \tag{14}$$

where C_{p_o} is the instantaneous, vibrational response of the sample to a temperature change. Creation, motion, and destructions of holes are cooperative, kinetic processes and may be slow. This leads to deviations from Eq. (14) if the measurement is carried out faster than the kinetics allows. Applied to the glass transition, one can write a simple, first-order kinetics expression to describe the time-dependent, apparent heat capacity in the glass-transition region [2]:

$$\left(\frac{dN}{dt}\right) = \frac{1}{\tau}(N^* - N) \tag{15}$$

where N represents the instantaneous number of holes, N^*, the equilibrium number of holes, and τ is the relaxation time for the formation of holes. Both, N^* and τ are dependent on temperature [2] and through Eq. (1) on time. Equation (15) can also be derived from other representations of the time dependence of the glass transition. Most general would be the use of irreversible thermodynamics. In this case $1/\tau$ is proportional to the curvature of the free energy relative to the relaxing internal variable at equilibrium [5]. Approximate solutions of Eq. (15), of use for various modes of TMDSC, have been discussed [12, 13]. The limits of applicability of Eq. (15) at larger distance from equilibrium involve the dependence of τ on N and deviations from the assumed simple exponential dependence of τ on temperature. A more detailed discussion of these limits and their possible correction with additional fitting parameters is given in Ref. [9].

For the present simulations, a numerical integration of Eq. (15) is used with the experimental temperature dependence of τ and N^* [9]. For the limited temperature range of the glass transition region, one can assume that both N^* and τ have an Arrhenius-type temperature dependence. The glass-transition range is then divided into time intervals, Δt, of one second, each with a constant N^* and an average value of τ. The value of N at the end of the one-second interval is given after integration over the one-second intervals by:

$$N_i = N_i^* - (N_i^* - N_{i-1})\, e^{-\Delta t/\sqrt{\tau_i \times \tau_{i-1}}} \tag{16}$$

with i representing the running index of time. Because of the one-second intervals, i equals t.

Figure 2 shows a sample calculation of N, N^*, and ΔN on cooling (A) and heating (B). On cooling the modulation freezes at a value of N that corresponds to the equilibrium number of holes at 340.34 K, the fictive temperature. Subsequent heating of the glass produced in the cooling some hysteresis behavior (Fig. 2B, enthalpy relaxation) [2, 7].

Using the heat flow $HF(t)=\Delta N\times\varepsilon_h$, with ΔN as shown in Fig. 2, one can calculate the various Fourier components of Eq. (10). With Eq. (3) one can then calculate the heat capacities corresponding to the total heat flow $<HF(t)>$ [component b_0 of Eq. (10)]. In Fig. 3, the heavier curves show this total heat capacity C_p(total). In the glass transition region there is still some evidence of periodic changes. A detailed analysis with larger modulation amplitudes has shown that this remaining effect, which is largely lost by further smoothing, is due to a small frequency shift of the modulation, resulting from the different time effects of the constant underlying cooling or heating rates and the modulation [10].

Equation (2) permits, next, to calculate the first harmonic response to the temperature modulation, using Eqs (4) to (9), as shown in Fig. 1. This represents the pseudo-isothermal evaluation by determining first $HF(t)$–b_0 and using the Fourier

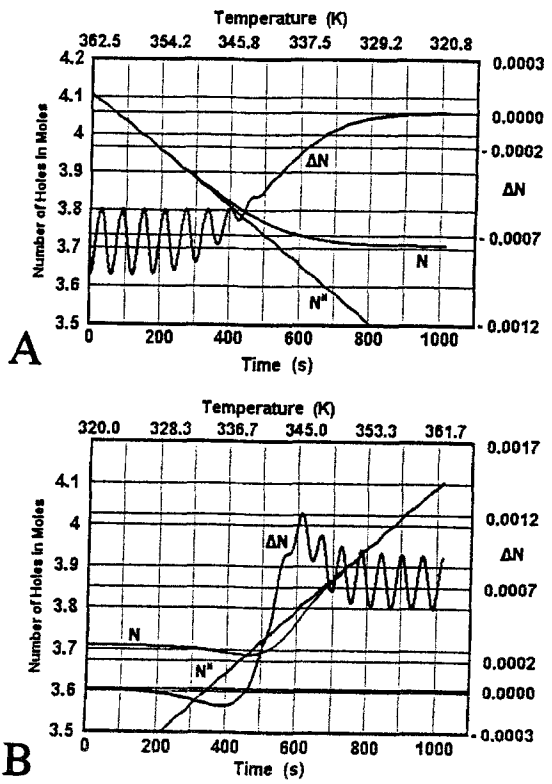

Fig. 2 Sample calculation of the changes of the equilibrium number of holes, N^*, the instantaneous number of holes, N, and the difference, ΔN. A, on cooling, B, on heating. The fictive temperature indicates at what temperature the equilibrium number of holes would be equal to N in the temperature region where $\Delta N=0$

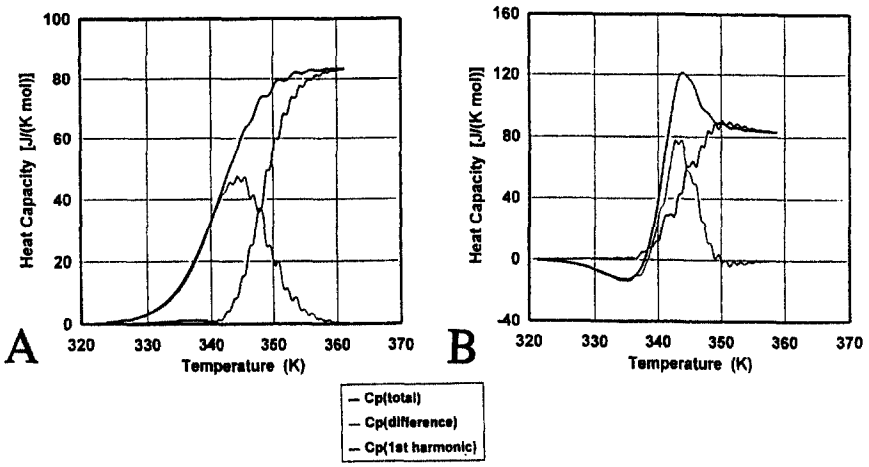

Fig. 3 Separation of the data of Fig. 2 into the total heat capacity, C_p(total), and first harmonic component ("reversing" heat capacity of the MDSC software), using the method illustrated in Fig. 1. The remaining modulation of the various curves is due to the frequency shift, caused by the interaction between underlying heating rate and modulation frequency [10]. A, on cooling, B, on heating

components a_1 and b_1, Eqs (12) and (13), for the calculation of A_Δ for Eq. (3). Figure 3 shows the example analyzed in Fig. 2. In the liquid temperature region (above 360 K) and in the glassy temperature region (below 320 K) the standard method of measurement of heat capacity of Eq. (3) and the pseudo-isothermal method of computation of the "reversing" heat capacity of Eq. (2) give the same values. In the intervening glass transition region, the time dependence must be considered.

Figure 4 illustrates that there is still a second harmonic response to the temperature modulation (based on the Fourier components a_2 and b_2). This second harmonic response represents only 2.8 and 4.5% of the total enthalpy integrated from 322.5 to 360 K for cooling and heating, respectively. The reason for a heat-capacity component with double the frequency of modulation is the faster relaxation time during the high-temperature portion of the cycle [12].

Even higher harmonics contribute even less to the heat capacity than the second harmonics (i.e. on cooling, the third harmonics reaches under the conditions of Figs 2 to 4 1.31% of the integrated total enthalpy change between 322.5 and 360 K, while the fourth harmonic reaches 0.9%). Much of these higher harmonic contributions beyond $\nu=2$ are linked to the frequency shift of the heat flow relative to the modulation. Comparison with the experimental data would require one further smoothing step that was omitted in the present calculation to discern the detailed glass transition effects.

Results

The input parameters for the simulations were derived from three sets of quasi-isothermal measurements of the glass transition of amorphous poly(ethylene terephthalate) (PET). The experiments are described [9] and the pertinent results are

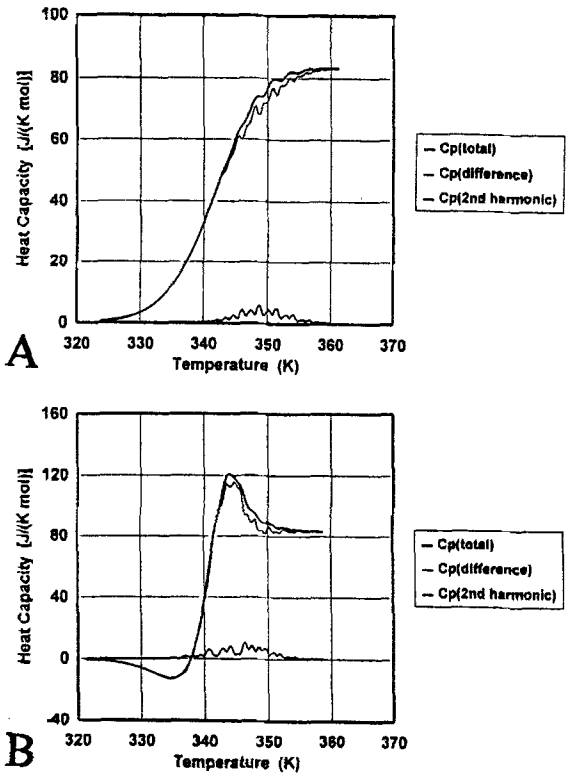

Fig. 4 Separation of the data of Fig. 2 into the total heat capacity and second harmonic component adapting the method illustrated in Fig. 1. A, on cooling, B, on heating

listed in Table 1. The measurements [9] were carried out quasi-isothermally between 320 and 390 K at intervals of 2 K with modulation periods of 30, 60 and 90 s and corresponding sample temperature amplitudes of 0.5, 1.0 and 1.5 K, respectively, so that the maximum heating rates were 6.3 K min^{-1} in all experiments. The activation energies derived for each set of experiments were then extrapolated to zero amplitude. Values for semicrystalline and drawn films are available [9].

First, the heat capacities corresponding to the first harmonic of the modulation at zero modulation amplitude were computed from the experimental data (reversing heat capacity signal, Fig. 3). The experimental activation parameters were used to extra-polate to modulation periods ranging from 0.01 to 120 s. The results are shown in Fig. 5.

Next, the change of number of holes with time at different modulation frequencies was calculated with the parameters of Table 1, and is illustrated for one example in Fig. 2. The underlying heating and cooling rates $<q>$ were chosen to be 2.5 K min^{-1} and the modulation period was varied from 10 to 120 s. The low modulation amplitude of 0.1 K was used to minimize the interference between the underlying heating rate and the modulation frequency, as discussed in Ref. [9]. Each cooling simulation was followed by heating. Cooling at 2.5 K min^{-1} yields a glass with 3.7105 moles of holes frozen in the glassy state when using the parameters of

Table 1 Input data for amorphous poly(ethylene terephthalate)

Property	Equation or value	Unit
Hole energy, ε_h	4700	J mol^{-1}
Equilibrium number of holes, N^*	19.53 exp($-\varepsilon_h/RT$)	mol
Activation energy ε_j	328,000	J mol^{-1}
$\varepsilon_j(t)$	5.59×10^{-49} exp(ε_j/RT)	second
Molar mass, MW	18,000	Da
ΔC_p at glass transition	84.164	J (K mol)$^{-1}$
Glass transition temperature, T_g	346.5	K
Repeating unit mass, M_o	192.2	Da

Table 1 (Fig. 2A). This corresponds to the equilibrium number of holes at a (fictive) temperature of 340.34 K. The changes in the number of holes is converted to the total reversing, first harmonic heat flow by the method illustrated in Fig. 1. Using Eqs (2) and (3) heat capacities were calculated, as shown in Fig. 3. Finally, the heat capacities were summed over the available full modulation cycles to approximate the involved enthalpies. Figure 1 shows that in the simulations without smoothing, data on A_Δ are available only one cycle after the first heat-flow value and one cycle before the last. While the simulations ran always between 320 and 362.5 K, the enthalpies could thus only be determined between somewhat shorter temperature ranges that differ for each chosen period. For example for $p=10$ s, the 1000 heat capacity amplitudes between 320.4 and 362.1 K were summed, divided by 1000, and multiplied with the temperature difference of 41.7 K. The results for all simulations are listed in Table 2.

The analysis of the dependence on modulation frequency was followed by a check of the change in freezing and unfreezing at a fixed modulation period of 20 s, but changing the underlying heating rate from 0.25 to 10.0 K min^{-1}. From curves as shown in Fig. 3 the glass transition temperatures were extracted at the point where half the change of heat capacity had occurred. Table 3 shows the data.

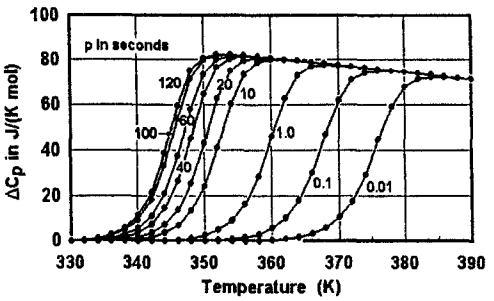

Fig. 5 Reversing heat capacity of poly(ethylene terephthalate) as a function of modulation period. Computed using quasi-isothermal data of Ref. [9] extrapolated to zero modulation amplitude

Finally, the enthalpy relaxation on heating was analyzed by simulating the heating of glasses with fictive temperatures from 350 to 325 K on heating at 2.5 K min^{-1}, at a modulation period of 20 s and an amplitude of 0.1 K. Table 4 shows the results, Fig. 3B an example.

Table 2 Frequency dependence of the enthalpy contributions

	Range of T/	Cooling		Heating	
p/s	K	H(tot)/J	H(1st harmonic/J	H(tot)/J	H(1st harmonic/J
10	320.4–362.1	1833	866	1830	917
20	320.8–361.7	1798	990	1795	1097
40	321.7–360.8	1728	1060	1726	1261
60	322.5–360.0	1659	1062	1757	1344
120	325.0–355.0	1337	887	1338	1555

Table 3 Dependence of the glass transition temperature in K on $<q>$*

$<q>$/ K min^{-1}	T_g from C_p (total) on cooling	T_g from C_p (1st harmonic) on cooling	T_g from C_p (1st harmonic) on heating
0.25	334.2	349.5	349.6
0.60	336.6	349.7	349.6
1.25	339.4	350.5	349.1
2.50	341.9	351.5	348.2
5.00	345.1	352.9	346.5**
10.0	349.2	355.5	342.6**

*The quasi-isothermal glass transition temperature at $p=20$ s is 349.3 K (Fig. 5)
**The hysteresis peak and the reversing C_p overlap.

Discussion

The simulation method illustrated in Figs 1 to 4 permits the detailed correlation of the effect of the kinetics of a slow process on the analysis of data by TMDSC. The key condition for the applicability of this analysis is that there is only a negligible temperature gradient within the sample and steady state is maintained during the modulation cycles. To get highest precision in kinetics, it may be necessary to use small sample masses and sample geometries that maximize heat transfer. The calorimeter most suitable for such analysis must have a quick response without sacrifice of the precision of temperature measurement. The assumed first order kinetics of Eq. (15) can easily be changed if more information about the particular process is available.

A comparison of Figs 2A and 3A shows that the modulation of the number of holes on cooling stops long before the slow approach to the fictive temperature is

Table 4 Dependence of the enthalpy contributions on the fictive temperature*

Fictive temp./K	Holes at time zero/mol	H(total)/J	H(1st harmonic)/J
350.0	3.885	974.0	1085.6
347.5	3.840	1186.3	1085.8
345.0	3.795	1397.7	1087.9
342.5	3.746	1628.0	1092.5
340.34	3.7105	1794.8	1097.3
337.5	3.659	2036.8	1105.9
335.0	3.614	2248.3	1114.5
332.5	3.568	2464.5	1123.7
330.0	3.522	2680.1	1133.2
327.5	3.477	2892.1	1142.6
325.0	3.431	3108.3	1152.3

$<q>=2.5$ K min^{-1}, $A=0.1$ K, $p=20$ s. The data are obtained by summing from 320.8 to 361.7 K, see Fig. 3B and Table 2. The cooling data are: H(tot)=1798.0; H(1st harmonic)= 989.8 J.

complete. As a result, the glass transition temperature extracted from the total heat flow is much lower (see also Table 3). The same is true for the heating (Figs 2B and 3B). The continuous approach to N^*, the enthalpy relaxation, starts much earlier than the modulation. Note that initially the enthalpy relaxation is exothermic, then it changes to endothermic. Comparisons with experiments [2, 10] revealed that at such distance from equilibrium (the liquid state) the first-order kinetics does not hold. The measured exotherm is much smaller than calculated, or not observable at all. It is hoped that analyses of the type presented here will help in devising a better mathematical description. A check of Figs 4A and B suggests that the second harmonic is rather small, so that the "reversing" heat capacity calculated with the MDSC software of TA Instruments [Eqs (4–9)] which represents only the first harmonic response is close to the full reversible effect, but still only an approximation.

Figure 5 is based on the experimental data extrapolated to zero modulation amplitude. Because of the fit of the relaxation time to an Arrhenius expression and the omission of consideration of the asymmetry of the approach to equilibrium at larger distance from equilibrium, it is likely that long extrapolations beyond the experimental frequency range of $p=30$–100 s are not valid [9], but may serve to establish the limit of the analysis presented in this paper.

The enthalpies calculated by summing the steps of the simulation show that, as expected, the total enthalpies on heating and cooling, H(tot), are equal, as required by the first law of thermodynamics. The remaining small differences of 1–3 J are due to the slight differences of the annealing trends included in the averaging that extends beyond the summations. The decrease in the total enthalpy on cooling and heating results exclusively from the decrease in temperature range of the summations. The heating and the cooling curves of C_p(total) shown in Figs 3A and B can be superimposed for the different modulation periods except for the small oscilla-

tions due to a minor frequency shift in the glass transition region, discussed in [9]. The glass transition temperature on cooling is 341.9 K (Table 3), much less than for the first harmonic (Fig. 5). The reason for this difference are the different time scales for the two measurements. The total heat flow that governs C_p(total) extends over the much longer annealing time available for the linear cooling experiment than for one modulation cycle (Fig. 2). A direct comparison of the glass transition of similar p and q, often attempted in comparing glass transitions from different analysis methods [1], is thus difficult. On heating, the temperature where C_p(total) has reached half its increase is not the glass transition since it does not correspond to the point of half-devitrification. The heat capacity value is obliterated by the enthalpy relaxation. A comparison of the T_g from the reversing heat capacity and the total heat capacity shows that on faster cooling, the two time scales interact, increasing T_g of the 1st harmonic as much as the T_g of C_p(total).

The "reversing" enthalpies should increase with increasing modulation period because of the shift of their glass transition to lower temperature, as shown in Fig. 5. For the heating experiments this is indeed the case (see the last column of Table 2). The difference between reversing enthalpy on cooling and heating, in turn, increases linearly with increasing modulation period p. It is zero at $p=0$, and 668 J at $p=120$ s. This difference of the "reversing" heat capacities on heating and cooling in the presence of an underlying heating rate $<q>$ was discussed in detail before [9]. The computation using Eq. (15) causes on cooling a shift of the apparent heat capacity to slightly higher temperature, and on heating, to lower temperature. The corresponding enthalpies in columns 4 and 6 document this change. Since the glass transition shifts on cooling with increasing p to lower temperature, and the integrated temperature interval decreases, one finds a maximum in column 4 of Table 2. This discrepancy between the "reversing" apparent heat capacities on cooling and heating decreases with smaller underlying heating rate. Table 3 shows that differences between cooling and heating disappear as one approaches quasi-isothermal experiments.

Table 4, finally, illustrates the increase in enthalpy relaxation contained in H(total) as the fictive temperature decreases. All values must be compared to H(total) on cooling (1798 J). High fictive temperatures, as can be obtained on fast cooling, lead to an exothermic enthalpy relaxation, low fictive temperatures show an overwhelming endothermic effect. For a fictive temperature of 340.34 K, corresponding in Table 4 to the same cooling and heating rates, the enthalpy relaxation approaches zero (equal amounts of exothermic contribution at low temperature and endothermic, at high temperature). One would expect that H(1st harmonic) on heating would not be affected by this enthalpy relaxation. As a first approximation this is the case, all values in Table 4 are close to 1097. Inspecting the detailed curves, as for example in Fig. 3B, one sees, however, that the strong changes during the minima and maxima in the total heat capacity add small Fourier components to the "reversing" heat flow [Eqs (4) to (13)]. An exotherm in the total heat flow adds enthalpy to the "reversing" heat flow, and an endotherm subtracts enthalpy. Below the fictive temperature of 340.34 K set on cooling, the deviations from 1097 J are accordingly negative, and above they are positive.

Conclusion

The simulation of the glass transition with a first order kinetics expression with parameters derived from quasi-isothermal experiments using TMDSC permit a discussion of the observed apparent heat capacities. The comparison of numbers of holes (Fig. 2) with apparent heat capacities (Figs 3 and 4) clarifies many of the observed effects and points to the limits of the present theory. The most pressing need is, as already pointed out in [2] to develop a cooperative kinetics expression for vitrification and devitrification beyond the present empirical expressions. The quantitative differences between experiment and computation, although small, may lead to progress.

* * *

This work was supported by the Division of Materials Research, National Science Foundation, Polymers Program, Grant # DMR 90-00520 and the Division of Materials Sciences, Office of Basic Energy Sciences, U. S. Department of Energy at Oak Ridge National Laboratory, managed by Lockheed Martin Energy Research Corp. for the U. S. Department of Energy, under contract number DE-AC05-96OR22464. Support for instrumentation came from TA Instruments, Inc. Research support was also given by ICI Paints, and Toray Industries, Inc.

References

1 See for example: S. Matsuoka, "Relaxation Phenomena in Polymers," Hanser Publ., Munich, 1992.
2 B. Wunderlich, D. M. Bodily and M. H. Kaplan, J. Appl. Phys., 35 (1964) 95.
3 M. Reading, D. Elliot and V. L. Hill, J. Thermal Anal., 40 (1993) 949; P. S. Gill, S. R. Sauerbrunn and M. Reading, ibid., 931; M. Reading, Trends in Polymer Sci., 8 (1993) 248.
4 B. Wunderlich, Y. Jin and A. Boller, Thermochim. Acta, 238 (1994) 277.
5 B. Wunderlich, "Thermal Analysis," Academic Press, Boston, MA, 1990.
6 B. Wunderlich, A. Boller, I. Okazaki and S. Kreitmeier, Thermochim. Acta, 283 (1996) 143.
7 A. Boller, C. Schick and B. Wunderlich, Thermochim. Acta, 266 (1995) 97.
8 A. Boller, Y. Jin and B. Wunderlich, J. Thermal Anal., 42 (1994) 307.
9 I. Okazaki and B. Wunderlich, Submitted to J. Polymer Sci., Part B: Polymer Phys., December issue (1996).
10 L. C. Thomas, A. Boller, I. Okazaki and B. Wunderlich, Thermochim. Acta to be published.
11 B. Wunderlich, to be published, J. Thermal Anal., (1996).
12 B. Wunderlich, A. Boller, I. Okazaki and S. Kreitmeier, Submitted to J. Thermal Anal. to be published.
13 A. Boller, I. Okazaki and B. Wunderlich, Thermochim. Acta, 284 (1996) 1.